Methanol to Olefins Reaction over Cavity-type Zeolite: Cavity Controls the Critical Intermediates and Product Selectivity

Wenna Zhang,[†,‡,⊥] Jingrun Chen,[†,⊥] Shutao Xu,[†] Yueying Chu,[§] Yingxu Wei,*[,†] Yuchun Zhi,[†] Jindou Huang,[†] Anmin Zheng,*[,§] Xinqiang Wu,[†,‡] Xiangju Meng,[∥] Fengshou Xiao,[∥] Feng Deng,[§] and Zhongmin Liu*[,†]

[†]National Engineering Laboratory for Methanol to Olefins, Dalian National Laboratory for Clean Energy, iChEM (Collaborative Innovation Center of Chemistry for Energy Materials), Dalian Institute of Chemical Physics, Chinese Academy of Sciences, Dalian 116023, P. R. China

[§]State Key Laboratory of Magnetic Resonance and Atomic Molecular Physics, National Center for Magnetic Resonance in Wuhan, Institute of Physics and Mathematics, Chinese Academy of Sciences, Wuhan 430071, P. R. China

[∥]Department of Chemistry, Zhejiang University, Hangzhou 310028, P. R. China

[‡]University of Chinese Academy of Sciences, Beijing 100049, P. R. China

Ⓢ *Supporting Information*

ABSTRACT: Methanol to olefins (MTO) reaction over H-RUB-50 zeolite, an eight-membered ring (8-MR) and cavity-type zeolite, presents higher selectivity for ethene. The host−guest interaction was dissected and used to explain the cavity-controlled reaction route and product selectivity. By the aid of the in situ ^{13}C MAS NMR spectroscopy, GC-MS, $^{12}C/^{13}C$-methanol switch experiments, and theoretical calculations, the methylbenzenium cations, methylcyclopentenyl cations (triMB$^+$, tetraMB$^+$, and triMCP$^+$), and their deprotonated forms with less methyl groups substitution were captured over LEV zeolite and confirmed as the critical reaction intermediates. The energetic span model was employed to identify the preferred reaction mechanism and provide the theoretical evidence to understand product selectivity.

The side-chain methylation mechanism was theoretically predicated to be the energetically favorable route for olefins generation with the participation of these active intermediates. Paring cycle with trimethlycyclopentadienyl cation as the intermediate makes less contribution to ethene formation due to the relatively large energy span. Based on the overall evaluation of the catalytic cycle, the difference of energy span of the whole reaction pathway for ethene and propene formation can give direct theoretical evidence for product selectivity. Additional study to the steps for generating precursors of ethene and propene offers extra support on the understanding of product selectivity and the dominant generation of ethene. This study captured the critical intermediates and established a rational and energetically feasible route of light olefins generation from MTO reaction over H-RUB-50. More importantly, it is exhibited that cavity controls the product selectivity via the important steric constraint for the formation of critical intermediates and the proceeding of critical reaction steps, based on the understanding of the host−guest interaction of the cavity-type zeolite catalyzed MTO reaction.

KEYWORDS: *methanol to olefins, H-RUB-50, critical intermediates, product selectivity, host−guest interaction, cavity-control*

1. INTRODUCTION

Methanol-to-olefins (MTO) reaction over zeolites and zeotype catalysts has become a successful process for light olefins production via nonpetrochemical route from the abundant resources of coal or natural gas.[1−3] The application of MTO technology, such as DMTO technology developed by Dalian Institute of Chemical Physics, has gained great economic profit since the first commercialization in Baotou, China in 2010.[3] Along with the industrialization of the MTO process, the understanding of the mechanism and the product selectivity control principle, serving as the basis for further optimizing the catalyst and reaction process, have drawn considerable research

interest.[4−9] In the past 40 years, great research efforts have been devoted to the core issue of the MTO reaction mechanism, the formation route of C−C bond from C1 reactant, by the aid of experimental studies[6,10−12] and theoretical calculations.[13−16] The MTO mechanism has undergone the evolution from direct mechanism[17] to indirect mechanism.[4,5,18,19] It is generally accepted that efficient MTO reaction proceeds via a rational and energetically feasible

pathway with an indirect mechanism,[4,18,19] and alkenes species[20−22] and aromatics species[10,23−27] act as the important intermediates or co-catalysts for the light olefins formation. Two distinct reaction routes of hydrocarbon-pool (HCP) mechanism, named side-chain methylation and paring routes, were proposed to explain product generation via the aromatics-based cycle.[10,28−30]

The capture and identification of the critical intermediates and their involvement in the MTO reaction are of great significance for the catalytic cycle establishment and reaction mechanism proposal. Benzenium and cyclopentenyl cations and their deprotonated forms have been identified as the active intermediates on zeolites and zeotype catalysts.[10,27,29,31−33] Heptamethylbenzenium, pentamethylcyclopentenyl cations, and their deprotonated forms were captured on the cavity-type catalysts (H-SAPO-34,[8] DNL-6,[27] H-SSZ-13[10]), and pentamethylbenzenium, di/trimethylcyclopentenyl cations, and heptamethylbenzenium cations behaved as the important reaction intermediates on H-ZSM-5[29] and H-Beta.[32,33] The critical intermediates capture and identification laid the foundation for the catalytic cycle establishment of olefins generation.

The reaction intermediates have been considered as the vital factor for regulating the product distribution.[34,35] Song[34] and Wang[35] suggested that methylbenzenes with less methyl groups favored ethene formation, whereas polymethylbenzenes with more methyl groups led predominantly to the generation of propene and higher olefins. Actually, olefin products are generated via a series of elementary reactions in the complicated catalytic cycles. Based on the comprehensive assessment of the critical intermediates and the catalytic cycles, rate-determining states and intermediates can be determined and rational strategies can be developed to realize the reaction control. In essence, the structure−performance relationship in MTO reaction, including the critical intermediates, reaction route, and product selectivity, originates from the host−guest interaction of the cavity-type zeolite catalyzed MTO reaction system. As a special catalysis of MTO reaction, the host−guest interaction determines the exact manner in which critical intermediates are formed and how they mediate the olefin products generation in the catalytic environment.

8-MR and cavity-type zeolites have drawn great attention due to their unique product selectivity for light olefin.[8,36,37] In some earlier studies, the selective olefin production in MTO reaction over H-SAPO-34 was ascribed to product shape selectivity in the catalyst with narrow eight-membered ring (8-MR) pore opening.[38,39] In our previous work, methanol reaction over SAPO catalysts[8] with very close 8-MR pore opening and varied cavity structure exhibited distinct methanol conversion and product distribution. The difference in product distribution cannot be explained by the product shape selectivity due to the very close pore opening. Instead, the cavity size[36] and spatial confinement effect[8] conferred by the cavity-type catalyst have been found to control the intermediates formation and furthermore dictate the product generation. To clarify the MTO reaction in the cavity-type catalysts and the cavity-controlled product selectivity, more deep understanding about this catalytic reaction system with strong host−guest interaction is required, including not only the critical intermediates formation but also the selective formation of some specific olefin products.

In the present work, MTO reaction was performed over H-RUB-50 zeolite, with 8-MR pore opening and small LEV

cavity. Cavity-controlled MTO reaction was studied as an example of host−guest interaction of zeolite-catalyzed reaction system. The reaction presents high light olefins selectivity, especially ethene selectivity, which is much higher than that over H-SSZ-13, H-SAPO-34, and DNL-6, the catalysts with almost identical 8-MR pore opening and relatively large supercage. By the aid of solid-state ^{13}C MAS NMR, critical intermediates, methylbenzenium and methylcyclopentyl cations, were first captured in LEV-type catalyst during the MTO reaction, and their significance in olefins generation was investigated by ^{12}C/^{13}C-methanol switch experiment and theoretical calculations. Employing the energetic span model, an energetically favorable catalytic cycle with the involvement of these intermediates was established to explain ethene and propene generation. The preference of ethene generation over H-RUB-50 with small cavity was evaluated by the comparison on the energy span of the whole catalytic cycle. The evaluation of the critical step, the generation of precursors of the olefin products, provides additional support to the product selectivity. A rational clarification of predominant ethene generation and cavity-controlled reaction was given based on the complete consideration of host−guest interaction of MTO reaction in cavity-type zeolite, including the critical intermediates formation, the catalytic cycle with the involvement of these intermediates, and the depression of bulky olefin precursor formation in H-RUB-50 zeolite.

2. EXPERIMENTAL SECTION

2.1. Catalyst and Characterizations. Na-RUB-50(Si/Al = 17) was synthesized following the procedure described in the literature.[40] H-RUB-50 was obtained through ion exchange with 1.0 mol L^{-1} NH$_4$NO$_3$ aqueous solution at 80 °C, followed by calcination at 550 °C for 4 h. The characterization results of powder X-ray diffraction (XRD) pattern, scanning electron microscope (SEM), N$_2$ adsorption, and NH$_3$-TPD experiments are detailed in Figures S1−S4 in the Supporting Information.

2.2. Catalytic Test. MTO reaction was performed in a fixed-bed quartz tubular reactor at atmospheric pressure. A catalyst sample of 100 mg was loaded into the reactor and activated in the flow of helium before reaction. The reactions were carried out at the temperature range of 275−400 °C. The methanol was fed by passing the carrier gas (He) through a methanol saturation evaporator maintained at 14 °C with the molar ratio of helium to methanol of 10 and WHSV of methanol of 2.0 h^{-1}. The effluent products from the reactor were kept warm and analyzed on online by gas chromatography (Agilent GC 7890A) equipped with a HP-PLOT Q capillary column and a FID detector.

For the ^{13}C MAS NMR spectroscopy measurement of the retained organics in the catalyst, methanol conversion was performed with ^{13}C-methanol as the reactant following the procedure mentioned above. ^{13}C-methanol was fed into the reactor for a predetermined time, and then the reactor was removed from the feeding line, and the catalyst was cooled very quickly by putting them into the vessel containing liquid nitrogen. Finally, the cooled catalyst was transferred to an NMR rotor in the glovebox without exposure to ambient air.

2.3. [12]C/^{13}C-Methanol Switch Experiment. In the ^{12}C/^{13}C-methanol switch experiment, the ^{12}C-methanol was fed by passing the carrier gas (He) through a methanol saturation evaporator maintained at 14 °C into the reactor at 300 °C for 25 min to build up ^{12}C-HCP species in the cavity of H-RUB-50. Then the feeding of ^{12}C-methanol was stopped,

and ^{13}C-methanol (fed by passing the carrier gas (He) through a ^{13}C-methanol saturation evaporator) was switched into the reactor for 1 min, and then the catalyst was cooled very quickly by putting it into the vessel containing liquid nitrogen. The isotopic distribution of effluents and the materials confined in the catalyst was analyzed using an Agilent 7890A/5975C GC/MSD.

2.4. Confined Organics Determination with GC–MS. Organic species retained in the spent H-RUB-50 catalyst after the MTO reaction were analyzed following the procedures as described in the literature.[41] The spent catalysts were dissolved in 20% hydrofluoric acid solution. The organic phase was extracted by dichloromethane (CH_2Cl_2). The extracted organics were then analyzed using an Agilent 7890A/5975C GC/MSD and identified by the mass spectral library of NIST08.

2.5. ^{13}C MAS NMR Spectroscopy. All the solid-state ^{13}C MAS NMR measurements were performed on a Bruker AvanceIII 600 spectrometer equipped with a 14.1 T wide-bore magnet using a 4 mm MAS probe. The resonance frequency was 150.9 MHz for ^{13}C nucleus. ^{13}C MAS NMR spectra were recorded using high-power proton decoupling with a spinning rate of 12 kHz; 2700 scans were accumulated with a $\pi/4$ pulse width of 1.8 μs and a 4 s recycle delay. The chemical shifts were referenced to adamantane with the upfield methine peak at 29.5 ppm.

3. THEORETICAL CALCULATION

3.1. Theoretical Calculation for ^{13}C Chemical Shifts. In the structure optimization and subsequent calculations of ^{13}C NMR parameters, the electron correlation effects were modeled using the generalized gradient approximation (GGA) proposed by Perdew, Burke, and Ernzerhof (PBE method). In order to accurately describe the interactions between the carbenium ions and zeolite framework, the DFT-D method was used in the structure optimization, and the couplings between the core and valence electrons were described by ultrasoft pseudopotentials. In addition, a plane-wave cutoff energy of 550 eV and a $2 \times 2 \times 2$ Monkhorst–Pack K point grid in the Dmol3 package were adopted to sample the Brillouin zone. Calculations of all NMR parameters were performed by the GIPAW method[42] using a $2 \times 2 \times 2$ Monkhorst–Pack K point grid and by expanding all wave functions in a plane-wave basis set at a definite cutoff energy of 550 eV. All $(\delta^{13}C)_{cal}$ were derived using the CASTEP-NMR module available in the Materials Studio package[43] based on the optimized structures of carbenium ions accommodation in the H-RUB-50 zeolite. The ^{13}C-calculated chemical shift were further converted to $(\delta^{13}C)_{cal}$ values, which were referred to the absolute shielding of benzene, namely, 127 ppm for the experimental values.

3.2. Theoretical Calculation for MTO Reaction Mechanism. For theoretical calculations, a 52T cluster model ($Si_{51}AlO_{82}H_{45}$) represents the structure of H-RUB-50 zeolite as shown in Figures S5, which was extracted from the crystallographic LEV structure. In the theoretical calculations for the extended zeolite model, the terminal Si–H was fixed at a bond length of 1.47 Å, oriented along the direction of the corresponding Si–O bond. The locations of acid sites were chosen at the 8-MR window, accessible for adsorbents and surrounded by maximum reaction space.[44] The substituted Al atom was placed at the T2 site of the crystallographic position during structural optimization.

The combined theoretical ONIOM method[45−47] was applied to predict the geometries of various adsorption structures and transition states (TS). During the structure optimization, ωB97XD hybrid density function with 6-31G(d,p) basis sets and semi-empirical AM1 were employed for optimizing geometries of the high-level and low-level layer. The ωB97XD method is the hybrid meta DFT developed by Chai and Head-Gordon, where implicitly accounts for empirical dispersion and can describe long-range dispersion interactions well with respect to the traditional DFT methods.[48] To preserve the integrity of the zeolite structure during the structure optimizations, the 8-MR window, $(SiO)_3$–Si–OH–Al–$(SiO)_3$ active center, and the adsorbed species in the high-level layer were relaxed while the rest of atoms were fixed in the low level at their crystallographic locations. To obtain highly accurate energies, the single-point energies were calculated at the level of ωB97XD/6-31G(d,p) on the basis of optimized structures. The frequency calculations were performed at the same level as geometry optimizations to check whether the saddle points exhibit the proper number of imaginary frequencies. Only a single imaginary frequency was observed for the transition state, and no imaginary frequency was observed for the adsorbed state.

In order to compare with the real MTO reaction condition at 300 °C, the intrinsic free energies barriers ($\Delta G^{\ddagger}$) for each elementary reaction in a completed reaction route were obtained from the ωB97XD/6-31G(d,p) total electronic energies and the thermal correction from the ωB97XD/6-31G(d,p):AM1 frequency calculations. The reference pressure for the calculations of free energies is an atmosphere. The energies reported here have been corrected for zero-point vibration energies. All density functional theory (DFT) calculations were performed with the Gaussian 09 package.[49]

To visualize the noncovalent interactions between the adsorbed organic species and the zeolite framework, the noncovalent interaction index approach, developed by Yang et al.,[50] was adopted. In this approach, the reduced density gradient (RDG), defined as $RDG(r) = 1/(2(3\pi^2)^{(1/3)})|\nabla\rho(r)|/(\rho(r)^{(4/3)})$, together with the electron density ρ, was used to distinguish the covalent and noncovalent interactions. The noncovalent interactions are located at the regions with low density and low RDG. The sign of the second largest eigenvalue ($\lambda 2$) of the electron density Hessian is helpful to distinguish bonded ($\lambda 2 < 0$) from nonbonded ($\lambda 2 > 0$) interactions. In addition, the sign of $\lambda 2$ can identify different types of noncovalent interactions: ($sign(\lambda 2)\rho < 0$, H-bonding interaction; $sign(\lambda 2)\rho \approx 0$, weak van der Waals (vdW) interaction; and $sign(\lambda 2)\rho > 0$, strong repulsive interaction). To reveal clearly the intermolecular noncovalent interaction between the adsorbed organic species and the zeolite framework, the intramolecular interactions are eliminated for the calculated RDG function. The functions RDG and $sign(\lambda 2)\rho$ were calculated with the Multiwfn software.[51]

4. RESULTS AND DISCUSSION

4.1. Methanol to Olefins Conversion and Product Distribution over H-RUB-50 Zeolite. Methanol conversion and product yield over H-RUB-50 at 300 °C are shown in Figure 1. The catalytic performances at the temperature range of 275−400 °C are shown in Figures S6−S7. At low temperatures of 275 and 300 °C, an obvious induction period and low conversion are observed, while at temperatures of 350
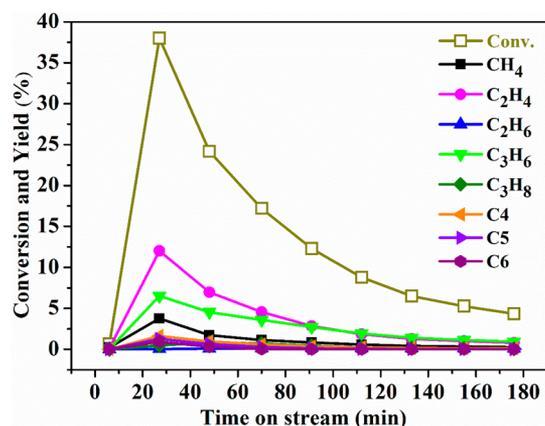
Figure 1. Methanol conversion and hydrocarbon product yields over H-RUB-50 catalyst with time on stream at 300 °C.

and 400 °C, complete methanol conversion is realized. With the increase of reaction temperature, methanol conversion is enhanced, while H-RUB-50 catalyst suffers from rapid deactivation as other catalysts with cavity structure and narrow 8-MR pore opening.[10,52,53] As shown in Figure 1, ethene and propene appear as the main products, especially ethene, which is quite different from the reaction over other cavity-type catalysts, such as H-SSZ-13,[10] H-SAPO-34,[52] and DNL-6,[8,53] where propene or butene are formed as the main products. During steady-state of methanol conversion at 300 °C over H-RUB-50, ethene/propene ratio (1.3−1.8) is higher than that from the reaction over other cavity-type catalysts (e.g., 0.6−0.75 over H-SAPO-34 at 300 °C),[52] which confirms cavity structure of zeolites varied the product generation. All these studies indicated that light olefins can be selectively generated, and the difference in the olefin products selectivity implies that the chemical environment of cavity-type catalyst plays a central role in determining the products distribution.

4.2. Carbenium Ions Capture and Identification by ^{13}C MAS NMR, GC−MS, and Theoretical Calculations.

The capture and identification of pivotal intermediates and the manner in which they are involved in methanol reaction are of great significance for the understanding of the mechanism. In the previous studies, experimental evidence confirmed the presence of benzenium and cyclopentenyl cations using ^{13}C MAS NMR spectroscopy and UV−vis spectroscopy,[8,10,29,30,54−56] such as pentamethylbenzenium, 1,3-dimethylcyclopentenyl, 1,3,4-trimethylcyclopentenyl, and ethylcyclopentenyl cations in H-ZSM-5[29,30,35,56] and heptamethylbenzenium cation, pentamethylcyclopentenyl cation in H-Beta,[32] DNL-6,[27] and H-SSZ-13,[10] noting that the carbenium ion speciation varies with the cavity dimension of the catalyst used. And in our previous work, it is found that carbenium ions are more stable in H-SSZ-13 with stronger Brønsted acidity than that in H-SAPO-34 with identical CHA cage for the carbenium ions accommodation.[10] The difference in carbenium ions formation and observation is possibly ascribed to acid strength of the Brønsted acid sites that are responsible for the protonation and stabilization of the intermediates in the catalysts. Besides the acidic property, the size and shape of the cavity of zeolite also play a crucial role in determining the reaction performance; thus, it is necessary to explore the host−guest interaction between cavity-type zeolite as the host and the intermediates as the guest in the MTO reaction. A representative ^{13}C MAS NMR spectrum of H-RUB-50 catalyst after methanol conversion at 300 °C for 25 min is given in Figure 2. The intensified signals are from alkylated aromatics (methylbenzenes, at 20, 120−140 ppm) and some diamondoid hydrocarbons (methyladamantanes, at 10−50 ppm), which are generated inside the cavity of the catalyst.[57,58] Besides the presence of these neutral organic species, some cations, i.e., polymethylcyclopentenyl cations (at 56, 155, 240−255 ppm) and polymethylbenzenium cations (at 144, 190, 203 ppm),[10] appear as well. Furthermore, the stability and precise structures
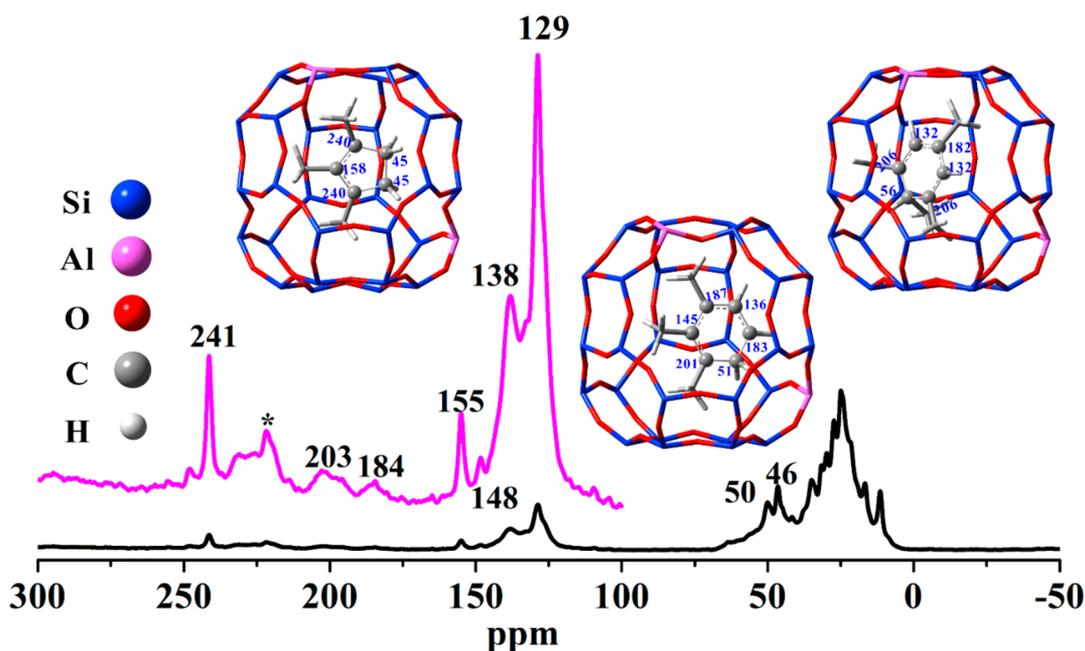
Figure 2. ^{13}C MAS NMR spectrum of retained organic species in H-RUB-50 after continuous-flow ^{13}C-methanol reaction at 300 °C for 25 min. The optimized structures of the triMCP$^+$, triMB$^+$, and tetraMB$^+$ cations confined in H-RUB-50 are given with calculated ^{13}C chemical shifts. The asterisk denotes spinning side-bands. The purple line is the enlarged spectra of the black line.

of these carbenium ions are theoretically assessed. As displayed in Table S2, the adsorption energies of polymethylbenzenium cations steadily increase with the concurrent increase of methyl group substitution, from −114.3 kcal/mol for trimethylbenzenium cation to −29.6 kcal/mol for heptamethylbenzenium cation, due to the increased repulsive force entailed by the confined cavity of H-RUB-50. In H-RUB-50, the carbenium ions with less methyl groups present higher stability, implying that their generation and accommodation in LEV cage are more energetically favorable. As depicted in Table 1,

Table 1. Calculated and Experimentally Measured ^{13}C Chemical Shifts of Carbenium Ions in H-RUB-50[a]

Carbenium ions	^{13}C chemical shifts	
	Calculated (ppm)	Experimental(ppm)
TriMCP$^+$	158 (C1)	155 (C1)
	240 (C2, C5)	241 (C2, C5)
	45(C3, C4)	46 (C3, C4)
TriMB$^+$	187 (C1)	184 (C1)
	145 (C2)	148 (C2)
	201 (C3)	203 (C3)
	51 (C4)	50 (C4)
	183 (C5)	184 (C5)
	136 (C6)	138 (C6)
TetraMB$^+$	182 (C1)	184 (C1)
	132 (C2, C6)	129 (C2, C6)
	206 (C3, C5)	203 (C3, C5)
	56 (C4)	50 (C4)

[a]The optimized structures of the triMCP$^+$, triMB$^+$, and tetraMB$^+$ cations confined in H-RUB-50 are shown in Figure 2 and Figure S8.

theoretical calculation predicts 1,2,5-trimethylcyclopentenyl cation with ^{13}C chemical shift at 45, 158, and 240 ppm, 1,2,3-trimethylbenzenium cation with ^{13}C chemical shift at 51, 136, 145, 187, and 201 ppm, and 1,3,4,5-tetramethylbenzenium cation with ^{13}C chemical shift at 56, 132, 182, and 206 ppm, respectively. The theoretical calculations of ^{13}C chemical shifts are in good agreement with the observations of ^{13}C MAS NMR spectroscopy. Hence, triMCP$^+$ (1,2,5-trimethylcyclopentenyl cation), triMB$^+$ (1,2,3-trimethylbenzenium), and tetraMB$^+$ (1,3,4,5-tetramethylbenzenium) cations are ascertained to be the essential reactive intermediates. Their optimized structures are presented in Figure 2 and Figure S8. In addition, the identification of the carbenium ions is also consolidated by the observation of the corresponding neutral species that is extracted from the spent catalyst and qualitatively analyzed by GC−MS method as shown in Figure S9. The detection of 1,2,3-trimethylcyclopentadiene, 1,2,3-trimethylbenzene, and 1,3,4,5-tetramethylbenzene, the deprotonated forms of triMCP$^+$, triMB$^+$, and tetraMB$^+$ carbenium ions in the GC−MS, is according to carbenium ions captured by ^{13}C MAS NMR, respectively. The peak at retention time of 8.6 min is ascribed to trimethylcyclopentadiene (triMCP), evidencing that five-membered ring carbenium ions are from the protonated form of triMCP (trimethylcyclopentenyl cation (triMCP$^+$)) formed and confined in LEV cavity. The signals at

retention time of 13.2 and 16.1 min representing 1,2,3-trimethylbenzene and 1,3,4,5-tetramethylbenzene also appear in the chromatograms of GC−MS, indicating the presence of methylbenzenium ions, trimethylbenzenium and tetramethylbenzenium. Therefore, the five-membered ring (triMCP$^+$) and six-membered ring (triMB$^+$ and tetraMB$^+$) cations have been successfully captured and directly observed in the H-RUB-50 zeolite under real MTO reaction conditions by employing the combined techniques of ^{13}C MAS NMR and GC−MS. The host−guest structure consisting of inorganic zeolite cage of H-RUB-50 and the accommodated carbenium ions would behave as a cocatalyst system to catalyze MTO reaction.

It is worthy to note that, even though methylcyclopenyl ions and methylbenzenium ions are formed in H-RUB-50 as the catalysts of H-SSZ-13[10] and DNL-6,[27] the confined carbenium ions and their corresponding neutral species in H-RUB-50 present less methyl groups substitution (Table 2), but rather,

Table 2. Intermediates Formed in MTO Reaction Catalyzed by the Typical 8-MR Zeotype Catalysts (e.g., SSZ-13,[10] DNL-6,[27,52] H-RUB-50)

	H-SSZ-13	DNL-6	H-RUB-50
	6.7 × 10 Å	11.4 × 11.4 Å	6.3 × 7.3 Å
Carbenium Ions			
Neutral Species			
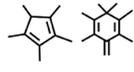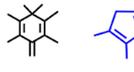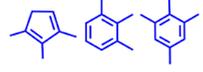
more methyl-groups-substituted heptamethylbenzenium cation and pentamethylcyclopentadienyl cation were observed over H-SSZ-13[10] with CHA topology (6.7 × 10 Å) and DNL-6[27,53] with RHO topology (11.4 × 11.4 Å) as given in Table 2. This illustrates that the large cavity structured CHA and RHO zeolite energetically allows the generation of bulky cyclopentenyl and phenylic intermediates, while the small cavity of H-RUB-50 favors the formation of less methyl-groups-substituted intermediates. The variation in the identity of the confined organic intermediates for distinct catalysts explicitly reflects the effect of cavity-controlled intermediates formation in the zeolite-catalyzed MTO reaction system with the strong host−guest interaction. It can be expected that the methanol conversion route and the selective formation of desired olefins would be controllable by changing the catalytic environment in zeolite cavity, based on the understanding of the host−guest interaction of MTO reaction system.

4.3. Reactivity of Confined Intermediates Determined by ^{12}C/^{13}C-Methanol Switch Experiments. To distinguish the reactive intermediates from the inert ones, ^{12}C/^{13}C-methanol isotopic switch experiment was employed to evaluate the reactivity of the retained organics in the catalyst. When the feeding is switched from ^{12}C- to ^{13}C-methanol, the interaction of methanol and reactive intermediates will give rise to more ^{13}C atoms incorporation. The isotopic scrambling in the olefin products and the confined organic species is compared in Figure 3. The generated olefin products contain ^{12}C and ^{13}C atoms, indicating that the retained organics are
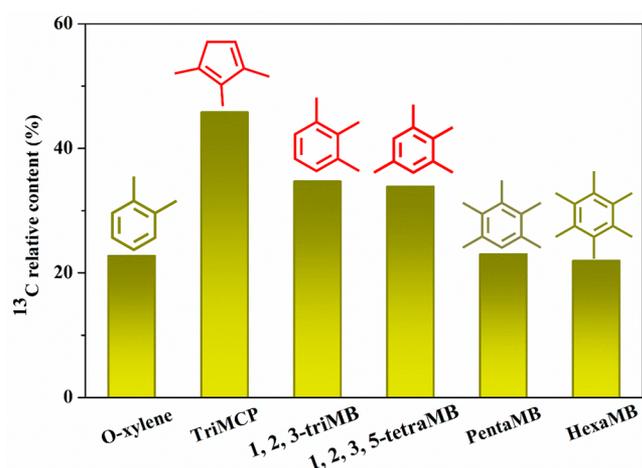
Figure 3. Relative ^{13}C content of the olefin products and the confined organic species in H-RUB-50 after ^{12}C-methanol reaction at 350 °C for 25 min followed by switching to ^{13}C-methanol for 1 min.

involved in olefin generation as well. Among the detected cyclic organics, 1,2,3-triMB, 1,2,3,5-tetraMB, and 1,2,3-triMCP exhibit higher ^{13}C contents than other components, implying the important role of these materials and their protonated forms as critical intermediates. It should be noted that the other isomers of triMB and tetraMB, such as 1,3,5-triMB, 1,2,4-triMB, and 1,2,4,5-tetraMB, possess relatively low reactivity; thus, the isomers structures matching well with the cavity structure of the zeolite would play a more important role. Even being formed in the cavity of H-RUB-50 catalyst, the reactivity of these confined cyclic organics and their role in MTO reaction are closely related with the steric constraint of small cavity structure in H-RUB-50. The cavity of the zeolite catalysts determines the formation and reactivity of the reaction intermediates based on the special host–guest interaction of the reaction system. Therefore, triMCP, triMB, and tetraMB with fewer methyl groups substituted were confirmed as active intermediates. All these intermediates can be formed through a series of secondary reactions, such as

oligomerization, cyclization, and hydride transfer during the induction period of MTO reaction.[54,59,60] For the methyl-benzenes, such as triMB and tetraMB, side-chain methylation mechanism has been suggested for their involvements in the olefins formation.[10,15,29,61] As an important five-ring inter-mediate, triMCP can lose H^- to cation (e.g., an alkoxy species ($C_3H_7^+$) derived from propene) to form trimethlycyclopenta-dienyl cation (1,2,5-triMCP$_{di}^+$).[54] This cyclopentadienyl cation (MCP_{di}^+) was widely regarded as a critical intermediate in the paring mechanism, which undergo ring contraction/expansion reactions to produce olefins.[10,28−30,54] The exact ways that they work will be discussed based on the establishment of the catalytic cycles with the intermediates participation and the complete analysis of the catalytic cycles with a series of elementary reactions in the next section.

4.4. Theoretical Study of Ethene Formation Routes: Catalytic Cycles of Side-Chain Methylation and Paring.
Experimental studies indicate that efficient methanol to olefins reaction is realized over H-RUB-50. Among the effluents products, ethene is predominantly formed with higher selectivity than other light olefin products. In the catalyst phase of H-RUB-50 catalyzed MTO reaction system, less-methyl-substituted MCP (methylcyclopentadiene), MB (meth-ylbenzene), and their protonated forms are captured, and their involvement in the reaction has been confirmed as the important intermediates of HCP mechanism. Based on these experimental observations and identification of triMCP (triMCP$_{di}^+$), triMB (triMB$^+$), and tetraMB (tetraMB$^+$), two reaction routes for ethene generation (Scheme 1, side-chain methylation and paring mechanisms) are suggested for theoretical evaluation.

During MTO reaction, water is also formed and adsorbed on Brφnsted acid site. Water participation promotes the proton shift between carbenium intermediates and bridge hydroxyl group[61,62] and may influence the acid-catalyzed elementary reaction steps. Thus in this work, in order to explore the influences of water on MTO reaction over H-RUB-50, all the elementary reactions in the catalytic cycle with/without the assistance of water were considered. The free energy barriers ($\Delta G^{\ddagger}$) of ethene formation at 300 °C via side-chain

Scheme 1. Full Catalytic Cycles of the Paring and Side-Chain Methylation Routes for the Formation of Ethene from Methanol Reaction over H-RUB-50[a]
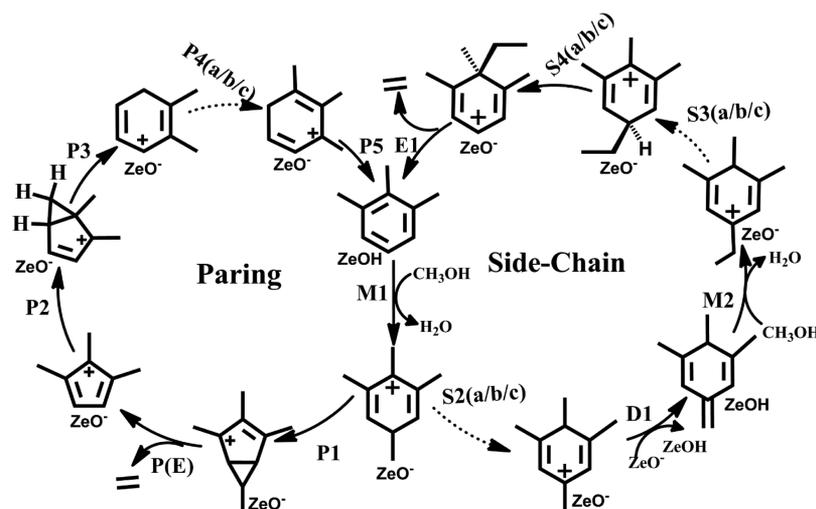
[a]The detailed pathway of S2 (a/b/c), S3 (a/b/c), S4 (a/b/c), and P4 (a/b/c) are shown in Scheme S1 in the Supporting Information.

methylation and paring routes assisted with water in methanol conversion over H-RUB-50 zeolite are depicted in Table 3, and

Table 3. Calculated Free Energy Barriers ($\Delta G^{\ddagger}$) at 300 °C of Ethene Formation via the Side-Chain and Paring Routes with the Assistance of Water in Methanol Conversion over H-RUB-50 Zeolite

side-chain route		paring route	
reaction steps	$\Delta G^{\ddagger}$ (kcal/mol)	reaction steps	$\Delta G^{\ddagger}$ (kcal/mol)
M1	37.01	M1	37.01
S2 (a/b/c)	19.49/21.60/4.48	P1	31.91
D1	11.27	P(E)	45.80
M2	23.15	P2	33.55
S3 (a/b/c)	12.32/9.07/15.59	P3	21.79
S4 (a/b/c)	10.30/19.19/10.66	P4 (a/b/c)	15.23/36.38/8.30
E1	15.52	P5	1.89

those without water assistance are listed in Table S3 in the Supporting Information. It is noted that water has different effects on different reaction types; taking the deprotonation and olefin elimination steps as examples, the free energy barriers could be effectively decreased with the assistance of water by 3−23 kcal/mol. In this way, water plays an important role as a bridge between the framework and the reaction intermediate.[61] However, Wang found that the addition of water may increase the free energy barrier of propene elimination step in MCM-22,[63] which is consistent with our results of propene elimination step in the next section (Table 4

Table 4. Comparison of the Calculated Free Energy Barriers ($\Delta G^{\ddagger}$) of the Elementary Reactions for Ethene and Propene Formation via Side-Chain Cycle at 300 °C with the Assistance of Water

cycle of ethene		cycle of propene	
reaction steps	$\Delta G^{\ddagger}$ (kcal/mol)	reaction steps	$\Delta G^{\ddagger}$ (kcal/mol)
M1	37.01	M1	37.01
S2(a/b/c)	19.49/21.60/4.48	S2(a/b/c)	19.49/21.60/4.48
D1	11.27	D1	11.27
M2	23.15	M2	23.15
S3(a/b/c)	12.32/9.07/15.59	D2	17.81
S4(a/b/c)	10.30/19.19/10.66	M3	36.43
E1	15.52	S5(a/b/c)	13.67/13.12/18.15
		S6(a/b/c)	3.17/2.47/6.74
		E2	13.52

and Table S5). All of these results illustrate that the influence of water is complex, which is related to the reaction types and zeolite structure. The roles of water need further study combining experimental technology and theoretical calculation in the future. Therefore, in this work, all of the reactions in the catalytic cycle with the assistance of water were considered and discussed as follows. In order to consider the effect of the basis sets on the calculations, single-point calculations of all the elementary reactions for ethene formation via side-chain cycle with the higher basis set of 6-311G (2df, 2p) were used to obtain energy values with high accuracy. The calculated results are listed in Table S4. The free energy barriers calculated by the higher basis sets (6-311G(2df,2p)) are very close to the values calculated by the previous basis set (6-31G(d,p)), and the theoretical errors are less than 1.5 kcal/mol for each step,

so the calculated free energy barriers were predicted using the basis set of 6-31G(d,p) as follows.

The reaction route of side-chain methylation mechanism is established based on the participation of the captured triMB$^+$ and tetraMB$^+$ carbenium ions, which starts from the methylation reaction (**M1**) of 1,2,3-trimethylbenzene (1,2,3-triMB) with methanol to form 1,2,4,6-tetramethylbenzenium (1,2,4,6-tetraMB$^+$) cation over Brønsted acid sites. Subsequently, in the side-chain methylation route (Scheme 1, right part), 1,2,4,6-tetraMB$^+$ cation is isomerized to the 1,3,4,5-tetraMB$^+$ cation by hydride transfer reaction (**S2a−c**). The following deprotonation of tetraMB$^+$ (**D1**) generates trimethylmethylenecyclohexadiene (TMMC) with exocyclic double bond, from which a benzenium cation with an ethyl side-chain group can be generated via the second methylation reaction (**M2**). Then the 3,4,5-trimethyl-1-ethylbenzenium (3,4,5-triM-1-EB) with ethyl side-chain group undergoes the hydride and ethyl group transfer (**S3**, **S4**) to form 3,4,5-trimethyl-4-ethylbenzenium (3,4,5-triM-4-EB) cation. With elimination reaction, ethene splits off (**E1**), and 1,2,3-triMB is regenerated. The Gibbs free energy profile at 300 °C of the catalytic cycles is shown in Figure 4, and the calculated free energy barriers are
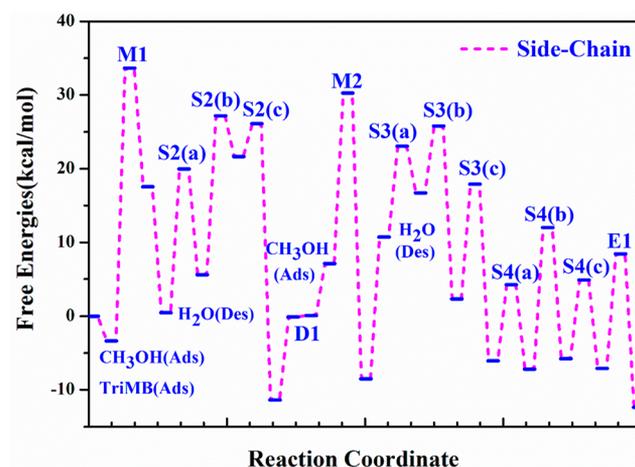
Figure 4. Gibbs free energy profile for methanol conversion to ethene over H-RUB-50 following the side-chain methylation route at 300 °C.

summarized in Table 3. In this cycle, the free energy barriers for two methylation steps (**M1**, **M2**) catalyzed with H-RUB-50 are 37.01 and 23.15 kcal/mol. The deprotonation reaction (**D1**) is a facile step with the free energy barriers of 11.27 kcal/mol. Three ethyl transfer steps of **S4(a)**, **S4(b)**, and **S4(c)** need to overcome free energy barriers of 10.30, 19.19, and 10.66 kcal/mol. The hydride transfers (**S2**, **S3** (Scheme S1)) and ethene elimination reactions (**E1**) in the cycle are more energetically feasible with free energy barriers in the range of 4.48−21.60 kcal/mol.

Ethene formation from methanol reaction via paring route is also considered for comparison (Scheme 1, left part). Starting from the methylation of 1,2,3-triMB, 1,2,4,6-tetraMB$^+$ cation is formed, which is then converted to 1,2,3,5-tetramethylbicyclo-[3.1.0] hexenyl cation via the step of ring contraction (**P1**), followed by the ethene elimination (**P(E)**) to generate ethene and 1,2,5-trimethylcyclopentadienyl cation (1,2,5-triMCP$_{di}$$^+$). Subsequently, the 1,2,5-triMCP$_{di}$$^+$ converts to dimethylbenzium (diMB$^+$) after the steps of hydride transfer (**P2**) and ring expansion (**P3**). The recovery of 1,2,3-triMB is

realized with a series of reaction steps, the deprotonation of diMB+ (**P4a**), methylation of diMB (**P4b**), hydride transfer (**P4c**), and deprotonation (**P5**) of triMB+. The Gibbs free energy profile of all the elementary steps of paring route at 300 °C is shown in Figure 5, and the calculated free energy barriers
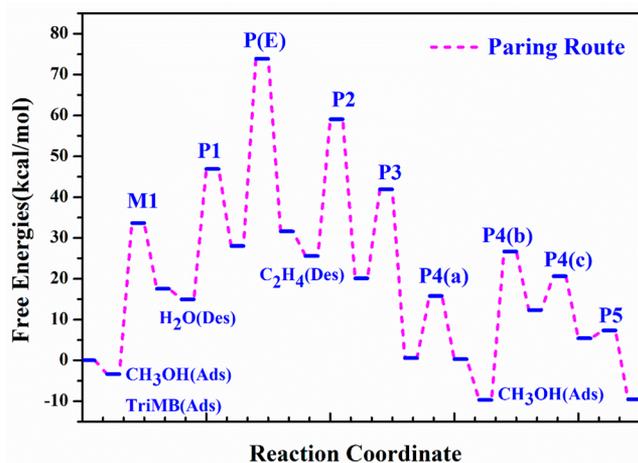
Figure 5. Gibbs free energy profile for methanol conversion to ethene over H-RUB-50 following the paring reaction route at 300 °C.

are summarized in Table 3. In the catalytic cycle of the paring route, the ring contraction step (**P1**) has the free energy barrier of 31.91 kcal/mol , and the elimination of ethene (**P(E)**) needs to overcome a higher free energy barrier of 45.80 kcal/mol. These free energy barriers are higher than that in the paring cycle starting from hexaMB as the critical intermediate in H-SSZ-13 (22.94 and 36.66 kcal/mol).[10] The hydride transfer (**P2**) and ring expansion (**P3**) are predicted with free energy barrier of 33.55 and 21.79 kcal/mol. The formed diMB+ goes through successive deprotonation (**P4a**, 15.23 kcal/mol), methylation (**P4b**, 36.38 kcal/mol), hydride transfer (**P4c**, 8.30 kcal/mol), and deprotonation (**P5**, 1.89 kcal/mol) steps to form 1,2,3-triMB intermediate to fulfill the catalytic cycle.

It is suggested and well-known that the catalytic reactivity is not only determined by the rate-determining step for the multistep reaction but also depends on the energetic span of the whole reaction. The energetic span model proposed by Shaik et al.[64] is a reliable method used to understand catalytic activity and selectivity of MTO reaction with complex pathway

with a series elementary reactions and variety of intermediates.[65,66] In this work, the energetic span model was employed to confirm the preferred reaction mechanism and provide theoretical evidence to understand product selectivity.

In the side-chain methylation mechanism, the rate-determining transition state is the methylation of trimethylmethylenecyclohexadiene (TMMC) with methanol (**M2**), and the most stable rate-determining intermediate is 1,3,4,5-tetraMB+ cation, which is in accordance with our experimental observation of tetraMB+ cation on ^{13}C MAS NMR. The energy span regarded as overall Gibbs energy barriers is around 41.62 kcal/mol in the side-chain methylation mechanism at 300 °C. In the paring mechanism, the ethene elimination (**P(E)**) is the rate-determining transition state, and the rate-determining intermediate is methanol and 1,2,3-triMB in adsorption. The energy span of paring mechanism (77.21 kcal/mol) is much higher than side-chain methylation mechanism by about 35.6 kcal/mol. From the energy span comparison of the side-chain methylation mechanism and paring mechanism, the side-chain methylation mechanism may be more dominant than the paring mechanism for ethene formation in the MTO reaction over H-RUB-50 zeolite. Larger energy span of paring cycle illustrates that this route with the involvement of triMCP$_{di}$+ has a weak contribution to ethene formation. Based on the calculation, such triMCP$_{di}$+ intermediate cannot be efficiently formed from the paring route. But for triMCP and triMCP+, due to the fact that they can be formed via other routes beside the paring cycle, especially formed via a series of secondary reactions, such as oligomerization, cyclization, and H-transfer of initial olefins products during the induction period of MTO reaction,[54,59,60] their formation can be verified by ^{13}C MAS NMR and GC−MS analysis.

From the complete catalytic cycle of the MTO reaction, besides the consideration of the energy span of the overall reaction cycle, the elementary steps, such as methylation and elimination steps, are very closely related with the catalytic activity. Specifically, as the critical steps, methylation (**M2**) in side-chain methylation and ethene elimination (**P(E)**) in the paring cycle present noticeable distinction in free energy barrier. The optimized transition states structures for the two critical steps are displayed in Figure 6. The methylation of TMMC with methanol (**M2**) in the side-chain methylation has lower energy barrier (23.15 kcal/mol) than the ethene elimination (**P(E)**) in the paring cycle (45.80 kcal/mol). This
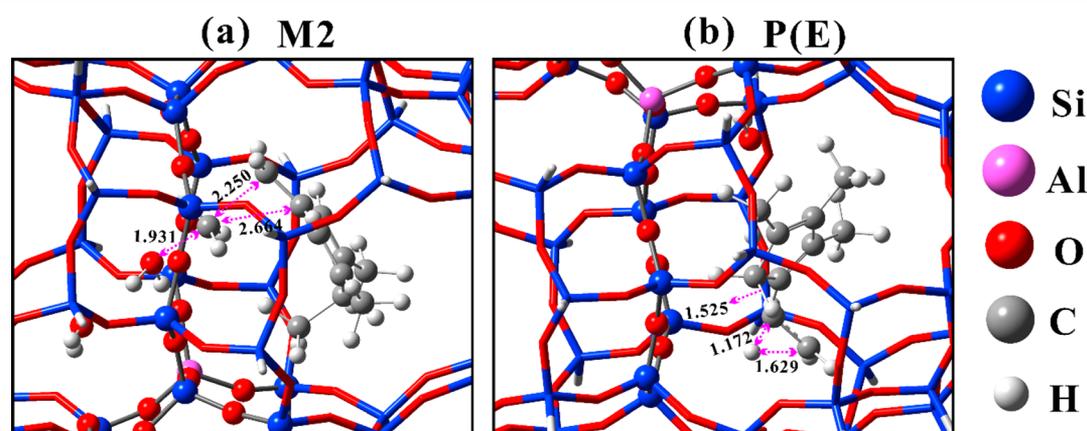
Figure 6. Optimized transition states structures for the critical steps of side-chain cycle (**M2**, (a)) and paring cycle (**P(E)**, (b)) for ethene formation over H-RUB-50.

result and the difference of the energy span clearly illustrate that the side-chain methylation reaction route with the involvement of methylbenzenium cations with less methyl groups as the important intermediates is more energetically favorable than the paring route for the formation of ethene over H-RUB-50. Therefore, the selective generation of olefin products on H-RUB-50 will be discussed based on the dominant pathway with side-chain methylation mechanism.

4.5. Cavity-Controlled Product Selectivity Derived from the Host−Guest Interaction. Selectivity control of methanol reaction for light olefins production, especially for some specifically wanted olefin products, is a great challenge in developing new MTO catalyst and MTO process. In the present work, when methanol reaction is performed over H-RUB-50, ethene prevails as the main product, presenting the considerable potential of LEV zeolite as an excellent MTO catalyst, especially for the production of ethene. Previous studies have proved that, by the usage of 8-MR and cavity-type catalysts, light olefins are the main products,[3,52] but the critical issue of shape selectivity, such as how the zeolite cavity structure dictates methanol reaction route of methanol to olefin reaction for the selective production of olefin products, has not been solved and understood sufficiently. One study of methanol reaction over the catalysts with the LEV, CHA, and AFX topology illustrated that the selectivity toward ethene increased when using the small-sized cavity catalyst.[36] Our previous work explored the MTO reaction over three types of silicoaluminophosphate (SAPO) molecular sieves with identical 8-MR pore opening and different cavities (SAPO-35 with LEV topology, SAPO-34 with CHA topology, and DNL-6 with RHO topology).[8] Comparable studies demonstrated that the product shape selectivity cannot explain the difference in product distribution due to the identical 8-MR pore opening for these three samples, and the cavity structure controlled the size and reactivity of confined organic species.[8] Unfortunately, still no definitive correlation has been established between the catalyst structure and selective generation of olefin products based on the consideration of the detailed reaction routes of MTO reaction at the molecular level. In this section, ethene and propene generation routes via side-chain methylation mechanism are constructed involving the complete catalytic cycles with all the elementary steps as depicted in Scheme 2. The formations of ethene and propene are examined theoretically and systematically from the view of the completely catalytic cycles with all the elementary steps.

Both ethene and propene formations are considered via the catalytic cycle of side-chain methylation with water assistance. As presented in Scheme 2, starting from triMB, the catalytic cycle of ethene generation proceeds through methylation over Brønsted acid site to generate tetraMB+, deprotonation to form TMMC (trimethylmethylenecyclohexadiene), and side-chain methylation to form the precursor of ethene, TMEB+ (3,4,5-trimethyl-1-ethylbenzenium). With a series of steps of hydride transfer (S3), ethyl side-chain group transfer (S4), and elimination (E1), ethene can be split off as the product. If the formed TMEB+ further proceeds deprotonation reaction (D2) to form TMEC (trimethylethylidenecyclohexadiene) with exocyclic double bond, then the propene precursor, the propylmethylbenzenium cation with propyl side-chain group (TMPB+, 3,4,5-trimethyl-1-propylbenzenium), can be formed via methylation reaction (M3) of the exocyclic bond of TMEC. Similar to the process of ethene formation, via a series of steps

Scheme 2. Catalytic Cycles for the Formation of Ethene and Propene through the Side-Chain Methylation Mechanism on H-RUB-50 Zeolite[a]
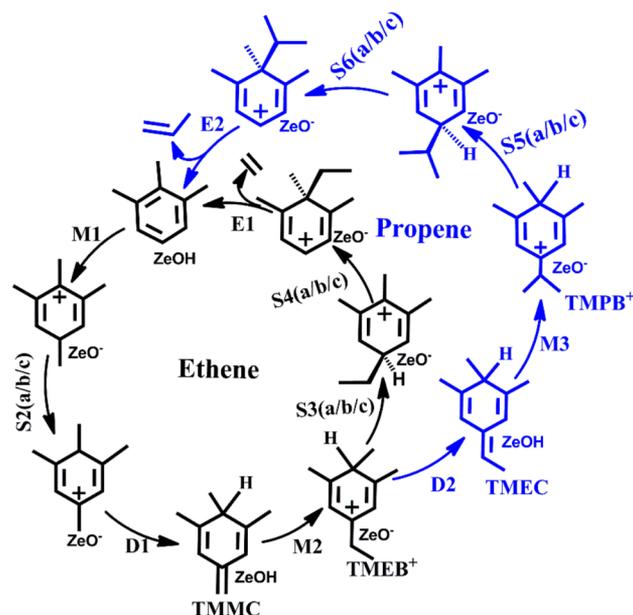
[a]The detailed pathways of **S5** (**a/b/c**) and **S6** (**a/b/c**) are shown in Scheme S2 in the Supporting Information.

of the hydride transfer (**S5**), propyl side-chain group transfer (**S6**), and elimination reaction (**E2**), propene splits off.

The details of the free energy barriers of all the elementary reactions at 300 °C for ethene and propene formation via side-chain methylation cycle are listed and compared in Table 4. The free energy barriers profiles are given in Figure 7. From
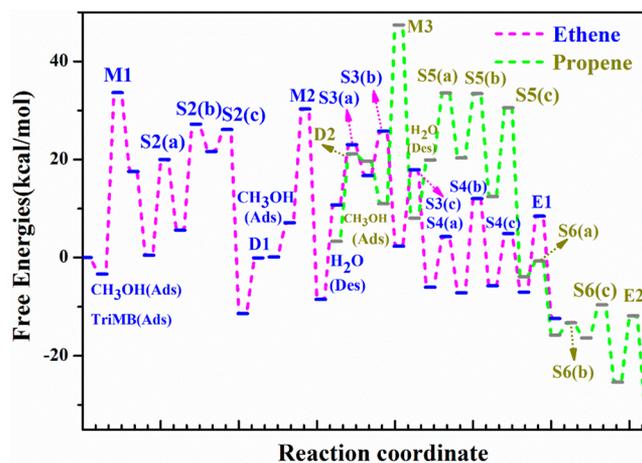
Figure 7. Gibbs free energy profiles of the formation of ethene and propene through the side-chain methylation mechanism on H-RUB-50 zeolite at 300 °C.

the complete cycle forming ethene and propene, the deprotonation steps to form exocyclic C═C double bond present relatively low free energy barrier, 11.27 kcal/mol for **D1** and 17.81 kcal/mol for **D2**, and two methylation steps (**M2** and **M3**) act as the key steps for forming ethene or propene precursor. The **M3** step, methylation of TMEC to form propene precursor, TMPB+, needs to overcome the free energy barrier of 36.43 kcal/mol, which is higher than the

value of the **M2** step (23.15 kcal/mol) for the formation of ethene precursor, TMEB$^+$, by 13.3 kcal/mol. Among other steps in the catalytic cycle of propene formation, similar to the reaction of ethene cycle, the hydride transfer (**S5**), propyl side-chain group transfer (**S6**), and elimination propene (**E2**) exhibit the low-energy barriers of 2.47−18.15 kcal/mol (Scheme S2). For the formation of propene, the rate-determining transition state is the side-chain methylation reaction (**M3**) of the TMEC (trimethylethylidenecyclohexadiene) with exocyclic bond; the most stable rate-determining intermediate is 1,3,4,5-tetraMB$^+$ cation adsorbed on zeolite. The energy span on the overall Gibbs free energy barriers for propene production is 58.78 kcal/mol, higher by 17.16 kcal/mol than that for ethene formation. This may explain the experimental observation of higher ethene selectivity in H-RUB-50. In this way, small cavity of H-RUB-50 zeolite imposes its host−guest interaction onto the rate-determining transition states and intermediates through increasing energy span of the overall reaction cycle for olefins formation.

Employing the energetic span model, the higher Gibbs free energy for propene production than that for ethene can give a direct theoretical prediction for selective product generation. It is worthy to note that in the HCP mechanism, the olefin generation is realized via the catalytic cycle with the growth of benzenium cation with alkyl side-chain by methylation and the followed elimination of side-chain to form the olefins. Moreover, for the ethene and propene formation in the catalytic cycle over H-RUB-50, the rate-determining transition states are the processes to generate benzenium cation with ethyl or propyl side-chain. Thus, additional study on the comparison of forming benzenium cation with alkyl side-chain, ethene and propene precursors, TMEB$^+$ and TMPB$^+$, will provide new insight into the selectivity control of the olefins product. The optimized structures for the formation of ethene and propene precursors are provided in Figure 8a. Compared

with ethene precursor generation, the formation of propene precursor with propyl side-chain group (**M3**) is predicted to overcome higher free energy barrier of 36.43 kcal/mol, while the formation of ethene precursor is of lower energy barrier (**M2**, 23.15 kcal/mol). Another consideration is that TMEB$^+$ is not only the precursor of ethene formation but also the starting material for propene generation. For the parallel reaction steps of TMEB$^+$ conversion, the energy barrier of hydride transfer of TMEB$^+$ (**S3**) is 12.32 kcal/mol in the ethene cycle, lower than the deprotonation step to form TMEC (**D2**) of 17.81 kcal/mol in the propene cycle. This also predicts that TMEB$^+$ tends to proceed via the reaction pathway for ethene formation rather than forming the bulky propene precursor. The difficulty for the formation of bulky propene precursor and the proceeding of propene cycle present the cavity-controlled reactions, which derives from the host−guest interaction of the intermediates and the zeolite catalyst. The theoretical prediction of energy span on the overall reaction cycle for olefins formation and the additional comparison of the formation of olefins precursors, for the first time, explain the difference of ethene and propene selectivity at the molecule level from the view of the complete catalytic cycle established for methanol to olefins reaction over H-RUB-50.

Figure 8a shows the geometries of the transition states of the methylation reaction to form TMEB$^+$, the precursor of ethene (**M2**), and TMPB$^+$, the precursor of propene (**M3**). For the methylation of trimethylmethylenecyclohexadiene (TMMC) to form TMEB$^+$ (Figure 8a1), the transition state structure of **M2** demonstrates the elongated C1−O1 bond with distance of 1.931 Å and a new C1−C2 bond formation at the side-chain, illustrating that carbon atom of methanol moves away from O1 of methanol to form a new C1−C2 bond (2.250 Å), and water generates simultaneously. At the same time, the TMEB$^+$ formation gives rise to the double bond of C2═C3 being elongated from 1.338 Å in the adsorbed TMMC to 1.364 Å in the transition state structure, indicating the generation of C2−C3 single bond. For the transition state structure of **M3**, the methylation of TMEC (the deprotonated form of TMEB$^+$) with methanol will generate the TMPB$^+$ cation (Figure 8a2), the precursor of propene. Figure 8b provides the isosurface plots of reduced density gradient for the transition states (TS) species for the formation of TMEB$^+$ (**M2**, (b1)) and TMPB$^+$(**M3**, (b2)) as the precursors of ethene and propene. The isosurface of the TS species forming TMPB$^+$ exhibits a large red region, indicating that it suffers a much stronger repulsive interaction from the zeolite framework compared with the TS species forming TMEB$^+$. The steric constraint imposed by the zeolite framework results in the pronounced repulsive interaction, and thus TS species displays a lesser stability, which accounts for the higher energy barrier for the TMPB$^+$ formation. The facile formation of the methylethyl-benzenium cation precursor compared to that of methyl-propylbenzenium cation precursor offers extra support to the ethene formation being superior to the propene formation. This confirms definitely from the molecular level that the chemical environment of LEV zeolite leads to the more preferentially selective formation of ethene than propene, based on the energy span of overall Gibbs free energies of the whole catalytic cycle for ethene or propene formation and the comparison of forming benzenium ions precursors with ethyl and propyl side-chain.

Cavity-type and 8-MR molecular sieve catalysts have been proved to be excellent MTO catalysts due to their delicate
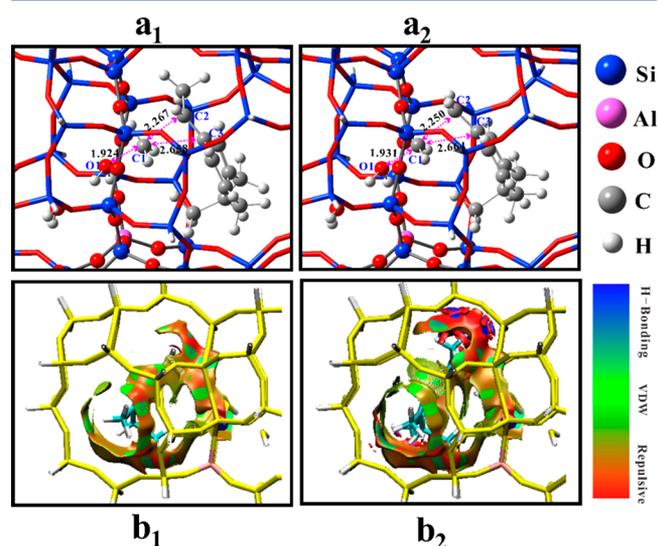
Figure 8. (a) Optimized transition state structures for the formation of TMEB$^+$ (3,4,5-trimethyl-1-ethylbenzenium) and TMPB$^+$ (3,4,5-trimethyl-1-propylbenzenium) as the precursors of ethene and propene through methylation reaction of (a1) **M2** and (a2) **M3**. (b) Isosurface plots of reduced density gradient for the transition states for the formation of TMEB$^+$ and TMPB$^+$ as the precursors of ethene and propene through methylation reaction of (b1) **M2** and (b2) **M3**.

structures with narrow pore opening prohibiting the diffusion out of aromatic compounds and some bulky hydrocarbons, and improving light hydrocarbons formation, especially light olefins generation as the target products. It is worthy to note that, even if these catalysts have identical 8-MR window, their catalytic performances, including the reactivity and product generation, differ with the topology of the catalyst.[8,10,25,27] Some relevant work illustrate the significance of the cavity structure and propose the cavity-controlled reaction.[8] It has been found that the reactivity and structure of the critical intermediates involved in the MTO reaction, such as the carbenium ions and their deprotonated-form compounds, vary with the chemical environment of the cavity-type catalyst, and the size and structure of the cavities determine the formation and function of these intermediates. For H-SSZ-13,[10] H-SAPO-34,[8] and DNL-6,[27,53] the catalysts with bulky-sized CHA or RHO type cavity, heptmethylbenzenium and pentamethylcyclopenyl cations, are the most important HCP species, and with their participation, MTO reaction is performed in a very efficient way. As for LEV type catalyst, H-SAPO-35 or H-RUB-50 studied in the previous work[8,36,37] and in the present study, MTO reaction is performed with the involvement of relatively small-sized intermediates, such as tetramethylbenzenium and trimethylcyclopentadienyl cations. The application of zeolite catalysts with different cavity structure alters the reaction performance to a great extent based on the strong host−guest interaction of MTO reaction system, via varying the critical intermediates formation and their involvement mode in the detailed reaction routes with the usage of cavity-type catalysts.

From the complete prospect of the MTO catalysis, besides the consideration of the energy span of the overall reaction cycle, the elementary steps, such as methylation, and elimination steps are very closely related with the target olefin product generation. Complete analysis of all these elementary reactions in the catalytic cycles would be helpful to understand the olefin products generation and clarify the nature of the selective generation of a certain olefin product through the proposed reaction pathway. In the confined catalytic environment, the reactions for the generation of olefins precursor with alkyl side-chain, such as methylethylbenzenium or methylpropylbenzenium cations through the methylation of methylmethylenecyclohexadiene or methylethylidenecyclohexadiene, as the critical steps for the olefin products generation, deserve special attention.

In our previous study of methanol reaction over H-SSZ-13 with CHA topology (6.7 × 10 Å), as shown in Figure S10 in the Supporting Information, the reaction to form methylethylbenzenium cation as the precursor of ethene needs to overcome the energy barrier of 23.13 kcal/mol, while the energy barrier for the further formation of methylpropylbenzenium cation as the precursor of propene with even bulky size is 17.58 kcal/mol.[10] This implies that the chemical environment of the CHA type zeolite energetically favors the generation of both of the two precursors. The space of the cavity structure of H-SSZ-13 can allow their formation through an even bulky transition state. For methanol reaction over LEV type zeolite, H-RUB-50, the formation of methylethylbenzenium cation as the precursor of ethene has lower free energy barrier (23.15 kcal/mol) than that of methylpropylbenzenium cation as the precursor of propene (36.43 kcal/mol). A more detailed study also confirms that the chemical surrounding of H-RUB-50 energetically favors the stabilization of methylethylbenzenium

cation with small-sized geometry, compared with methylpropylbenzenium cation (the adsorption energies are listed in Table S6). As the critical step of olefin generation through the reaction route of side-chain methylation, ethene and propene precursor formations present opposite case over the catalyst with CHA (6.7 × 10 Å) or LEV (6.3 × 7.3 Å) type cavity. In addition, Wang found that the energy span for ethene formation (196 kJ/mol) is similar to propene based on 1,2,4,5-TMB in side-chain methylation mechanism over H-SAPO-34 with CHA type cavity at 673 K.[65] Comparatively in the present work, the overall Gibbs free energy barrier for propene production in H-RUB-50 is higher by 17.16 kcal/mol (71.73 kJ/mol) than that for ethene formation. This also reflects the special catalysis with shape selectivity in MTO reaction over cavity-type zeolites. For the first time, the difference of the energy span of the overall catalytic cycle and the comparison of the formation of olefins precursors are verified and can be used to illuminate the predominant formation of certain olefin products over different cavity-type zeolite or zeotype catalysts. It is also the first time ascribing the shape selectivity concept of MTO reaction to the host−guest interaction of the cavity-type zeolite catalyzed MTO reaction system at the molecular level. The local environment of the 8-MR and cavity-type zeolite determines the shape selectivity of MTO reaction by controlling the formation of bulky intermediates, the proceeding of catalytic cycle, and the critical elementary reaction of the detailed reaction route.

5. CONCLUSION

H-RUB-50, an 8-MR and cavity-type zeolite, presents great potential as the catalyst for MTO reaction, especially for the ethene production. The critical intermediates, methylbenzenium cations, methylcyclopentenyl cations, and their deprotonated forms with less methyl groups substitution, were first captured during the reaction and identified using ^{13}C MAS NMR and GC−MS spectroscopies. With the participation of these identified active intermediates, the catalytic cycles of side-chain methylation and paring were established as ethene formation routes. Based on the energetic span model, theoretical calculation suggests that paring route with trimethlycyclopentadienyl cation involvement has a weak contribution to olefins production due to larger energy span, and side-chain methylation cycle is energetically favorable route for olefins formation. The difference of the energy span on overall energy barrier of the whole catalytic cycle and the comparison of the crucial steps for the formation of ethene and propene precursors rationalize the predominant formation of ethene as the main olefin product. Based on the special host−guest interaction of methanol conversion in the cavity-type and 8-MR zeolite catalyst, cavity structure of zeolite catalysts not only determines the formation of the critical intermediates and their involvement in the reaction routes but, ultimately, determines the reaction and selective product generation in MTO reaction.

■ ASSOCIATED CONTENT

ⓢ Supporting Information

The Supporting Information is available free of charge on the ACS Publications website at DOI: 10.1021/acscatal.8b02164.

Experimental and theoretical calculation details, catalyst characterization, and additional results (PDF)

AUTHOR INFORMATION

Corresponding Authors
*E-mail: liuzm@dicp.ac.cn (Z.L.).
*E-mail: weiyx@dicp.ac.cn (Y.W.).
*E-mail: zhenganm@wipm.ac.cn (A.Z.).

ORCID
Anmin Zheng: 0000-0001-7115-6510
Xiangju Meng: 0000-0001-8740-2755
Fengshou Xiao: 0000-0001-9744-3067
Feng Deng: 0000-0002-6461-7152
Zhongmin Liu: 0000-0001-8439-2336

Author Contributions
[⊥]W.Z. and J.C. contributed equally to this work.

Notes
The authors declare no competing financial interest.

ACKNOWLEDGMENTS

REFERENCES

(1) Chang, C. D.; Silvestri, A. J. The Conversion of Methanol and Other O-Compounds to Hydrocarbons over Zeolite Catalysts. *J. Catal.* **1977**, *47*, 249–259.

(2) Olsbye, U.; Svelle, S.; Bjorgen, M.; Beato, P.; Janssens, T. V.; Joensen, F.; Bordiga, S.; Lillerud, K. P. Conversion of Methanol to Hydrocarbons: How Zeolite Cavity and Pore Size Controls Product Selectivity. *Angew. Chem., Int. Ed.* **2012**, *51*, 5810–5831.

(3) Tian, P.; Wei, Y.; Ye, M.; Liu, Z. Methanol to Olefins (MTO): From Fundamentals to Commercialization. *ACS Catal.* **2015**, *5*, 1922–1938.

(4) Dahl, I. M.; Kolboe, S. On the Reaction Mechanism for Propene Formation in the MTO Reaction over SAPO-34. *Catal. Lett.* **1993**, *20*, 329–336.

(5) Kolboe, S.; Dahl, I. M. Methanol Conversion to Hydrocarbons. Use of Isotopes for Mechanism studies. *Stud. Surf. Sci. Catal.* **1995**, *94*, 427–434.

(6) Ilias, S.; Bhan, A. Mechanism of the Catalytic Conversion of Methanol to Hydrocarbons. *ACS Catal.* **2013**, *3*, 18–31.

(7) Hemelsoet, K.; Van der Mynsbrugge, J.; De Wispelaere, K.; Waroquier, M.; Van Speybroeck, V. Unraveling the Reaction Mechanisms Governing Methanol-to-Olefins Catalysis by Theory and Experiment. *ChemPhysChem* **2013**, *14*, 1526–1545.

(8) Li, J.; Wei, Y.; Chen, J.; Xu, S.; Tian, P.; Yang, X.; Li, B.; Wang, J.; Liu, Z. Cavity Controls the Selectivity: Insights of Confinement Effects on MTO Reaction. *ACS Catal.* **2015**, *5*, 661–665.

(9) Xu, S.; Zhi, Y.; Han, J.; Zhang, W.; Wu, X.; Sun, T.; Wei, Y.; Liu, Z. Advances in Catalysis for Methanol-to-Olefins Conversion. *Adv. Catal.* **2017**, *61*, 37–122.

(10) Xu, S.; Zheng, A.; Wei, Y.; Chen, J.; Li, J.; Chu, Y.; Zhang, M.; Wang, Q.; Zhou, Y.; Wang, J.; Deng, F.; Liu, Z. Direct Observation of Cyclic Carbenium Ions and Their Role in the Catalytic Cycle of the Methanol-to-Olefin Reaction over Chabazite Zeolites. *Angew. Chem., Int. Ed.* **2013**, *52*, 11564–11568.

(11) Wang, C.; Wang, Q.; Xu, J.; Qi, G.; Gao, P.; Wang, W.; Zou, Y.; Feng, N.; Liu, X.; Deng, F. Direct Detection of Supramolecular Reaction Centers in the Methanol-to-Olefins Conversion over Zeolite H-ZSM-5 by ^{13}C-^{27}Al Solid-State NMR Spectroscopy. *Angew. Chem., Int. Ed.* **2016**, *55*, 2507–2511.

(12) Wu, X.; Xu, S.; Zhang, W.; Huang, J.; Li, J.; Yu, B.; Wei, Y.; Liu, Z. Direct Mechanism of the First Carbon-Carbon Bond Formation in the Methanol-to-Hydrocarbons Process. *Angew. Chem., Int. Ed.* **2017**, *56*, 9039–9043.

(13) Van Speybroeck, V.; Hemelsoet, K.; Joos, L.; Waroquier, M.; Bell, R. G.; Catlow, C. R. Advances in Theory and Their Application within the Field of Zeolite Chemistry. *Chem. Soc. Rev.* **2015**, *44*, 7044–7111.

(14) Lesthaeghe, D.; Van Speybroeck, V.; Marin, G. B.; Waroquier, M. Understanding the Failure of Direct C-C Coupling in the Zeolite-Catalyzed Methanol-to-Olefin Process. *Angew. Chem., Int. Ed.* **2006**, *45*, 1714–1719.

(15) Arstad, B.; Nicholas, J. B.; Haw, J. F. Theoretical Study of the Methylbenzene Side-Chain Hydrocarbon Pool Mechanism in Methanol to Olefin Catalysis. *J. Am. Chem. Soc.* **2004**, *126*, 2991–3001.

(16) Wang, C.-M.; Wang, Y.-D.; Xie, Z.-K. Insights into the Reaction Mechanism of Methanol-to-Olefins Conversion in HSAPO-34 from First Principles: Are Olefins Themselves the Dominating Hydrocarbon Pool Species? *J. Catal.* **2013**, *301*, 8–19.

(17) Stöcker, M. Methanol-to-Hydrocarbons: Catalytic Materials and Their Behavior. *Microporous Mesoporous Mater.* **1999**, *29*, 3–48.

(18) Dahl, I. M.; Kolboe, S. On the Reaction Mechanism for Hydrocarbon Formation from Methanol over SAPO-34 0.1. Isotopic Labeling Studies of the Co-reaction of Ethene and Methanol. *J. Catal.* **1994**, *149*, 458–464.

(19) Dahl, I. M.; Kolboe, S. On the Reaction Mechanism for Hydrocarbon Formation from Methanol over SAPO-34 0.2. Isotopic Labeling Studies of the Co-reaction of Propene and Methanol. *J. Catal.* **1996**, *161*, 304–309.

(20) Dessau, R. M.; Lapierre, R. B. On the Mechanism of Methanol Conversion to Hydrocarbons over HZSM-5. *J. Catal.* **1982**, *78*, 136–141.

(21) Dessau, R. M. On the H-ZSM-5 Catalyzed Formation of Ethylene from Methanol or Higher Olefins. *J. Catal.* **1986**, *99*, 111–116.

(22) Dai, W.; Wang, C.; Yi, X.; Zheng, A.; Li, L.; Wu, G.; Guan, N.; Xie, Z.; Dyballa, M.; Hunger, M. Identification of Tert-Butyl Cations in Zeolite H-ZSM-5: Evidence from NMR Spectroscopy and DFT Calculations. *Angew. Chem., Int. Ed.* **2015**, *54*, 8783–8786.

(23) Bjorgen, M.; Svelle, S.; Joensen, F.; Nerlov, J.; Kolboe, S.; Bonino, F.; Palumbo, L.; Bordiga, S.; Olsbye, U. Conversion of Methanol to Hydrocarbons over Zeolite H-ZSM-5: On the Origin of the Olefinic Species. *J. Catal.* **2007**, *249*, 195–207.

(24) Arstad, B.; Kolboe, S. The Reactivity of Molecules Trapped within the SAPO-34 Cavities in the Methanol-to-Hydrocarbons Reaction. *J. Am. Chem. Soc.* **2001**, *123*, 8137–8138.

(25) Arstad, B.; Kolboe, S. Methanol-to-hydrocarbons Reaction over SAPO-34. Molecules Confined in the Catalyst Cavities at Short Time on Stream. *Catal. Lett.* **2001**, *71*, 209–212.

(26) Svelle, S.; Joensen, F.; Nerlov, J.; Olsbye, U.; Lillerud, K. P.; Kolboe, S.; Bjorgen, M. Conversion of Methanol into Hydrocarbons over Zeolite H-ZSM-5: Ethene Formation is Mechanistically Separated from the Formation of Higher Alkenes. *J. Am. Chem. Soc.* **2006**, *128*, 14770–14771.

(27) Li, J.; Wei, Y.; Chen, J.; Tian, P.; Su, X.; Xu, S.; Qi, Y.; Wang, Q.; Zhou, Y.; He, Y.; Liu, Z. Observation of Heptamethylbenzenium Cation over SAPO-type Molecular Sieve DNL-6 under Real MTO Conversion Conditions. *J. Am. Chem. Soc.* **2012**, *134*, 836–839.

(28) McCann, D. M.; Lesthaeghe, D.; Kletnieks, P. W.; Guenther, D. R.; Hayman, M. J.; Van Speybroeck, V.; Waroquier, M.; Haw, J. F. A Complete Catalytic Cycle for Supramolecular Methanol-to-Olefins Conversion by Linking Theory with Experiment. *Angew. Chem., Int. Ed.* **2008**, *47*, 5179–5182.

(29) Wang, C.; Chu, Y.; Zheng, A.; Xu, J.; Wang, Q.; Gao, P.; Qi, G.; Gong, Y.; Deng, F. New Insight into the Hydrocarbon-Pool Chemistry of the Methanol-to-Olefins Conversion over Zeolite H-ZSM-5 from GC-MS, Solid-State NMR Spectroscopy, and DFT Calculations. *Chem. - Eur. J.* **2014**, *20*, 12432–12443.

(30) Wang, C.; Yi, X.; Xu, J.; Qi, G.; Gao, P.; Wang, W.; Chu, Y.; Wang, Q.; Feng, N.; Liu, X.; Zheng, A.; Deng, F. Experimental Evidence on the Formation of Ethene through Carbocations in Methanol Conversion over H-ZSM-5 Zeolite. *Chem. - Eur. J.* **2015**, *21*, 12061−12068.

(31) Song, W. G.; Haw, J. F.; Nicholas, J. B.; Heneghan, C. S. Methylbenzenes are the Organic Reaction Centers for Methanol-to-Olefin Catalysis on HSAPO-34. *J. Am. Chem. Soc.* **2000**, *122*, 10726−10727.

(32) Bjorgen, M.; Bonino, F.; Kolboe, S.; Lillerud, K. P.; Zecchina, A.; Bordiga, S. Spectroscopic Evidence for a Persistent Benzenium Cation in Zeolite H-beta. *J. Am. Chem. Soc.* **2003**, *125*, 15863−15868.

(33) Zhang, M.; Xu, S.; Li, J.; Wei, Y.; Gong, Y.; Chu, Y.; Zheng, A.; Wang, J.; Zhang, W.; Wu, X.; Deng, F.; Liu, Z. Methanol to Hydrocarbons Reaction over H*β* Zeolites Studied by High Rresolution Solid-state NMR Spectroscopy: Carbenium Ions Formation and Reaction Mechanism. *J. Catal.* **2016**, *335*, 47−57.

(34) Song, W. G.; Fu, H.; Haw, J. F. Supramolecular Origins of Product Selectivity for Methanol-to-Olefin Catalysis on HSAPO-34. *J. Am. Chem. Soc.* **2001**, *123*, 4749−4754.

(35) Wang, C.; Xu, J.; Qi, G.; Gong, Y.; Wang, W.; Gao, P.; Wang, Q.; Feng, N.; Liu, X.; Deng, F. Methylbenzene Hydrocarbon Pool in Methanol-to-Olefins Conversion over Zeolite H-ZSM-5. *J. Catal.* **2015**, *332*, 127−137.

(36) Bhawe, Y.; Moliner-Marin, M.; Lunn, J. D.; Liu, Y.; Malek, A.; Davis, M. Effect of Cage Size on the Selective Conversion of Methanol to Light Olefins. *ACS Catal.* **2012**, *2*, 2490−2495.

(37) Li, P.; Zhang, W.; Han, X.; Bao, X. A Comparative Study of Methanol to Olefins over SSZ-13 and RUB-50 Zeolites. *Chin. J. Catal.* **2011**, *32*, 293−298.

(38) Chen, D.; Moljord, K.; Fuglerud, T.; Holmen, A. The Effect of Crystal Size of SAPO-34 on the Selectivity and Deactivation of the MTO Reaction. *Microporous Mesoporous Mater.* **1999**, *29*, 191−203.

(39) Hereijgers, B. P. C.; Bleken, F.; Nilsen, M. H.; Svelle, S.; Lillerud, K.-P.; Bjørgen, M.; Weckhuysen, B. M.; Olsbye, U. Product Shape Selectivity Dominates the Methanol-to-Olefins (MTO) Reaction over H-SAPO-34 Catalysts. *J. Catal.* **2009**, *264*, 77−87.

(40) Yamamoto, K.; Ikeda, T.; Onodera, M.; Muramatsu, A.; Mizukami, F.; Wang, Y.; Gies, H. Synthesis and Structure Analysis of RUB-50, an LEV-type Aluminosilicate Zeolite. *Microporous Mesoporous Mater.* **2010**, *128*, 150−157.

(41) Guisnet, M.; Costa, L.; Ribeiro, F. R. Prevention of Zeolite Deactivation by Coking. *J. Mol. Catal. A: Chem.* **2009**, *305*, 69−83.

(42) Profeta, M.; Mauri, F.; Pickard, C. J. Accurate First Principles Prediction of ^{17}O NMR Parameters in SiO_2 Assignment of the Zeolite Ferrierite Spectrum. *J. Am. Chem. Soc.* **2003**, *125*, 541−548.

(43) *Materials Studio 6.0*; Accelrys Inc.: San Diego, CA, 2012.

(44) O'Malley, P. J.; Dwyer, J. Ab-initio Molecular Orbital Calculations on the Siting of Aluminium in the Theta-1 Framework: Some General Guidelines Governing the Site Preferences of Aluminium in Zeolites. *Zeolites* **1988**, *8*, 317−321.

(45) Chu, Y.; Han, B.; Zheng, A.; Deng, F. Influence of Acid Strength and Confinement Effect on the Ethylene Dimerization Reaction over Solid Acid Catalysts: A Theoretical Calculation Study. *J. Phys. Chem. C* **2012**, *116*, 12687−12695.

(46) Lesthaeghe, D.; De Sterck, B.; Van Speybroeck, V.; Marin, G. B.; Waroquier, M. Zeolite Shape-selectivity in the Gem-methylation of Aromatic Hydrocarbons. *Angew. Chem., Int. Ed.* **2007**, *46*, 1311−1314.

(47) Papayannis, D. K.; Papavasileiou, K. D.; Melissas, V. S. Investigation of Bromine Atom Transfer Mechanism from an Alkyl Bromide Molecule to an O-bonded Alkyl Group in a FAU Zeolite by the ONIOM Method. *Microporous Mesoporous Mater.* **2016**, *226*, 1−9.

(48) Chai, J. D.; Head-Gordon, M. Long-range Corrected Hybrid Density Functionals with Damped Atom-atom Dispersion Corrections. *Phys. Chem. Chem. Phys.* **2008**, *10*, 6615−6620.

(49) Frisch, M. J.; Trucks, G. W.; Schlegel, H. B.; Scuseria, G. E.; Robb, M. A.; Cheeseman, J. R.; Scalmani, G.; Barone, V.; Mennucci, B.; Petersson, G. A.; Nakatsuji, H.; Caricato, M.; Li, X.; Hratchian, H. P.; Izmaylov, A. F.; Bloino, J.; Zheng, G.; Sonnenberg, J. L.; Hada, M.;
Ehara, M.; Toyota, K.; Fukuda, R.; Hasegawa, J.; Ishida, M.; Nakajima, T.; Honda, Y.; Kitao, O.; Naka, H.; Vreven, T.; Montgomery, J. A.; Peralta, J. E.; Ogliaro, F.; Bearpark, M.; Heyd, J. J.; Brothers, E.; Kudin, K. N.; Staroverov, V. N.; Kobayashi, R.; Normand, J.; Raghavachari, K.; Rendell, A.; J. Burant, C.; Iyengar, S. S.; Tomasi, J.; Cossi, M.; Rega, N.; Millam, J. M.; Klene, M.; Knox, J. E.; Cross, J. B.; Bakken, V.; Adamo, C.; Jaramillo, J.; Gomperts, R.; Stratmann, R. E.; Yazyev, O.; Austin, A. J.; Cammi, R.; Pomelli, C.; Ochterski, J. W.; Martin, R. L.; Morokuma, K.; Zakrzewski, V. G.; Voth, G. A.; Salvador, P.; Dannenberg, J. J.; Dapprich, S.; Daniels, A. D.; Farkas, O.; Foresman, J. B.; V.Ortiz, J.; Cioslowski, J.; Fox, D. J. *Gaussian 09*, revision B.01; Gaussian, Inc.: Wallingford, CT, 2010.

(50) Johnson, E. R.; Keinan, S.; Mori-Sanchez, P.; Contreras-Garcia, J.; Cohen, A. J.; Yang, W. Revealing Noncovalent Interactions. *J. Am. Chem. Soc.* **2010**, *132*, 6498−6506.

(51) Lu, T.; Chen, F. Multiwfn: a Multifunctional Wavefunction Analyzer. *J. Comput. Chem.* **2012**, *33*, 580−592.

(52) Chen, J.; Li, J.; Wei, Y.; Yuan, C.; Li, B.; Xu, S.; Zhou, Y.; Wang, J.; Zhang, M.; Liu, Z. Spatial Confinement Effects of Cage-type SAPO Molecular Sieves on Product Distribution and Coke Formation in Methanol-to-Olefin Reaction. *Catal. Commun.* **2014**, *46*, 36−40.

(53) Li, J.; Wei, Y.; Xu, S.; Tian, P.; Chen, J.; Liu, Z. Heptamethylbenzenium Cation Formation and the Correlated Reaction Pathway during Methanol-to-Olefins Conversion over DNL-6. *Catal. Today* **2014**, *226*, 47−51.

(54) Haw, J. F.; Nicholas, J. B.; Song, W. G.; Deng, F.; Wang, Z. K.; Xu, T.; Heneghan, C. S. Roles for Cyclopentenyl Cations in the Synthesis of Hydrocarbons from Methanol on Zeolite Catalyst HZSM-5. *J. Am. Chem. Soc.* **2000**, *122*, 4763−4775.

(55) Wulfers, M. J.; Jentoft, F. C. The Role of Cyclopentadienium Ions in Methanol-to-Hydrocarbons Chemistry. *ACS Catal.* **2014**, *4*, 3521−3532.

(56) Wang, C.; Sun, X.; Xu, J.; Qi, G.; Wang, W.; Zhao, X.; Li, W.; Wang, Q.; Deng, F. Impact of Temporal and Spatial Distribution of Hydrocarbon Pool on Methanol Conversion over H-ZSM-5. *J. Catal.* **2017**, *354*, 138−151.

(57) Pehk, T.; Lippmaa, E.; Sevostjanova, V. V.; Krayuschkin, M. M.; Tarasova, A. I. ^{13}C NMR Spectra of Adamantane Derivatives. *Org. Magn. Reson.* **1971**, *3*, 783−790.

(58) Wang, W.; Jiang, Y. J.; Hunger, M. Mechanistic Investigations of the Methanol-to-Olefin (MTO) Process on Acidic Zeolite Catalysts by *in situ* Solid-state NMR Spectroscopy. *Catal. Today* **2006**, *113*, 102−114.

(59) Qi, L.; Wei, Y.; Xu, L.; Liu, Z. Reaction Behaviors and Kinetics during Induction Period of Methanol Conversion on H-ZSM-5 Zeolite. *ACS Catal.* **2015**, *5*, 3973−3982.

(60) Wu, X.; Xu, S.; Wei, Y.; Zhang, W.; Huang, J.; Xu, S.; He, Y.; Lin, S.; Sun, T.; Liu, Z. Evolution of C-C Bond Formation in the Methanol-to-Olefins Process: From Direct Coupling to Autocatalysis. *ACS Catal.* **2018**, *8*, 7356−7361.

(61) De Wispelaere, K.; Hemelsoet, K.; Waroquier, M.; Van Speybroeck, V. Complete Low-barrier Side-chain Route for Olefin Formation during Methanol Conversion in H-SAPO-34. *J. Catal.* **2013**, *305*, 76−80.

(62) Wang, S.; Chen, Y.; Wei, Z.; Qin, Z.; Ma, H.; Dong, M.; Li, J.; Fan, W.; Wang, J. Polymethylbenzene or Alkene Cycle? Theoretical Study on Their Contribution to the Process of Methanol to Olefins over H-ZSM-5 Zeolite. *J. Phys. Chem. C* **2015**, *119*, 28482−28498.

(63) Wang, S.; Wei, Z.; Chen, Y.; Qin, Z.; Ma, H.; Dong, M.; Fan, W.; Wang, J. Methanol to Olefins over H-MCM-22 Zeolite: Theoretical Study on the Catalytic Roles of Various Pores. *ACS Catal.* **2015**, *5*, 1131−1144.

(64) Kozuch, S.; Shaik, S. How to Conceptualize Catalytic Cycles? The Energetic Span Model. *Acc. Chem. Res.* **2011**, *44*, 101−110.

(65) Wang, C.-M.; Wang, Y.-D.; Du, Y.-J.; Yang, G.; Xie, Z.-K. Similarities and Differences between Aromatic-based and Olefin-based Cycles in H-SAPO-34 and H-SSZ-13 for Methanol-to-Olefins Conversion: Insights from Energetic Span Model. *Catal. Sci. Technol.* **2015**, *5*, 4354−4364.

(66) Wang, C.-M.; Wang, Y.-D.; Du, Y.-J.; Yang, G.; Xie, Z.-K. Computational Insights into the Reaction Mechanism of Methanol-to-Olefins Conversion in H-ZSM-5: Nature of Hydrocarbon Pool. *Catal. Sci. Technol.* **2016**, *6*, 3279−3288.